



Article

Concentrated, Gradient Electrolyte Design for Superior Low-Temperature Li-Metal Batteries

Jason S. Packard, Ethan A. Adams and Vilas G. Pol *

Davidson School of Chemical Engineering, Purdue University, West Lafayette, IN 47907, USA

* Correspondence: vpol@purdue.edu

Abstract: Improving the low-temperature performance of lithium-ion batteries is critical for their widespread adoption in cold environments. In this study, we designed a novel LHCE featuring a solvent polarity gradient, designed to maximize both room- and low-temperature ion mobility. Extremely polar fluoroethylene carbonate (FEC) and low-freezing-point, $-135\text{ }^{\circ}\text{C}$, non-polar non-aflurobutyl methyl ether (NONA) were supplemented by two intermediate solvents with incremental step-downs in polarity. The intermediate solvents consist of methyl (2,2,2-trifluoroethyl) carbonate (FEMC) and either diethylene carbonate (DEC), ethyl methyl carbonate (EMC), or dibutyl carbonate (DBC). The four solvents were combined with 1 M lithium bis(fluorosulfonyl)amide (LiFSI) salt and were able to accommodate 37.5% diluent volume, resulting in ultra-low electrolyte freezing points below $-120\text{ }^{\circ}\text{C}$. This contrasts with our previously investigated three-solvent LHCE, which only allowed for a 14% diluent volume and a $-85\text{ }^{\circ}\text{C}$ freezing point. Localized high salt concentrations were shown by less than 3% of FSI- anions being free in solution. The gradient LHCEs also showed room-temperature ionic conductivities above 10–3 S/cm and maintained high ion mobility below $-40\text{ }^{\circ}\text{C}$. Lithium metal coin cells with LiFePO₄ (LFP) cathodes featuring the gradient LHCEs, a reference three-solvent LHCE, and commercial (1 M LiPF₆ in 1:1 EC:DEC) electrolyte were constructed. All gradient LHCEs outperformed both the three-solvent and commercial electrolytes at all temperatures, with the DEC-based gradient LHCE showing the best performance of 159.7 mAh/g at 25 $^{\circ}\text{C}$ and 109.2 mAh/g at $-50\text{ }^{\circ}\text{C}$, corresponding to a 68% capacity retention. These findings highlight the potential of LHCE systems to improve battery performance in low-temperature environments and propose a new gradient design strategy for electrolytes to yield advantages of both polar and weakly polar solvents.



Citation: Packard, J.S.; Adams, E.A.; Pol, V.G. Concentrated, Gradient Electrolyte Design for Superior Low-Temperature Li-Metal Batteries. *Batteries* **2024**, *10*, 448. <https://doi.org/10.3390/batteries10120448>

Academic Editor: Shaokun Chong

Received: 21 November 2024

Revised: 13 December 2024

Accepted: 17 December 2024

Published: 18 December 2024



Copyright: © 2024 by the authors. Licensee MDPI, Basel, Switzerland. This article is an open access article distributed under the terms and conditions of the Creative Commons Attribution (CC BY) license (<https://creativecommons.org/licenses/by/4.0/>).

1. Introduction

Since their commercialization in 1991, lithium-ion batteries (LIBs) have profoundly impacted society. Their high-energy density and long life cycles have proliferated the portable electronics, electric vehicle, and battery grid storage industries, and now play an imperative role in the transition to sustainable energy [1]. Despite their incremental improvement, typical LIBs with ethylene carbonate (EC) electrolytes suffer from poor low-temperature performance and lose over 50% of their room-temperature capacity at $-20\text{ }^{\circ}\text{C}$ [2–5]. To improve low-temperature performance, often LIB packs are maintained within a narrow, optimal temperature range using a thermal management system [6] or provide polyethylene glycol cooling solvent circulation around the battery pack. These methods increase cost, reduce energy density, and are insufficient for more extreme environments. The development of intrinsic material solutions is necessary to enable the mass adoption of sustainable energy technologies in harsh climates.

Limited low-temperature performance of LIBs arises primarily from sluggish cell kinetics including, reduced electrolyte ionic conductivity [7,8], high resistances for charge

transfer [9,10] and solid electrolyte interface (SEI) diffusion processes [8,11]. Strategies to increase ionic conductivity and decrease charge transfer and Li⁺ diffusion resistances through electrolyte modifications have been extensively studied. High salt concentration electrolytes (HCE) have been shown to create advantageous anion-derived SEIs, which lower interfacial resistances [12–15]. However, increasing the salt concentration increases viscosity and decreases ionic conductivity, limiting ultra-low-temperature performance. Locally high-concentrated electrolytes (LHCEs) are a promising method to maintain the superior anion-derived SEIs of HCEs while lowering viscosity and increasing ionic conductivity by adding an electrochemically inert, low-polarity and freezing-point co-solvent [16–21].

LHCE studies have often used coordinating solvents with moderate polarity, such as acetonitrile (AN), 1,2-dimethoxyethane (DME), or tetrahydrofuran (THF) [18,20]. Although advantageous for low-temperature performance, through improved desolvation and anion participation in the solvation shell, these lower polarity solvents limit ionic conductivity and performance at ambient temperatures. This problem could potentially be addressed by maximizing the polarity of coordinating solvent, while minimizing diluent polarity, to maintain low-temperature performance. This could allow for room-temperature ion mobility comparable to standard EC-based LIB electrolytes, while the diluent severely lowers the solution freezing point, viscosity and allows for anion participation in the solvation shell. Our recent work investigated this strategy using very polar fluoroethylene carbonate (FEC), methyl 2,2,2-trifluoroethyl carbonate (FEMC), and nearly non-polar nonafluorobutyl methyl ether (NONA) in a 2:4:1 ratio with 1 M Lithium bis(fluorosulfonyl)imide (LiFSI) salt [22]. This LHCE showed a freezing point of -85°C and 61% retention of room-temperature capacity at -50°C for Li-metal cells. However, creating an electrolyte solution with such a stark difference in polarity of its solvents gives rise to miscibility issues, analogous to mixing oil and water. The LHCE was limited to only 14% diluent by volume; a further reduction in freezing point and increase in low-temperature performance could have been achieved through greater diluent incorporation. In this work, we developed a gradient LHCE, featuring three different coordinating solvents, each with an incremental drop in polarity. This step-down design of solvent polarity allows for maximum miscibility and 37.5% incorporation of the diluent, despite using very polar FEC and non-polar NONA.

2. Materials and Methods

2.1. Materials

Fluoroethylene carbonate (FEC) was purchased from Acros Organics, Antwerp, Belgium. Methyl-2,2,2-trifluoroethyl carbonate (FEMC) was obtained from Synquest Labs, Alachua, FL, USA. Polyvinylidene fluoride (PVDF) polymer was purchased from Alfa Aesar, Ward Hill, MA, USA. The COM electrolyte, which included 1 M LiPF₆ in 1:1 v/v% EC:DEC, nonafluorobutyl methyl ether (NONA), N-Methyl-2-pyrrolidone (NMP), lithium bis(fluorosulfonyl)imide (LiFSI), and Lithium bis(trifluoromethanesulfonyl)imide (LiTFSI), was purchased from Sigma Aldrich, Waukesha, WI, USA. Lithium iron phosphate (LFP) was purchased from Sigma Aldrich. Chemicals were used as purchased without further purification.

2.2. Electrolyte Synthesis

The experimental electrolytes were synthesized in an argon-filled glovebox, NEXUS II Vacuum Atmospheres Co. (Hawthorne, CA, USA), with oxygen concentrations below 1.0 ppm and water concentrations below 0.5 ppm. Solvents were first measured and stirred in previously mentioned ratios at room temperature in vials. Then, salts were added in 1 M concentrations and stirred until a homogenous mixture was formed. Electrolytes were stored in the glove box and out of light at room temperature.

2.3. Electrode and Coin Cell Fabrication

LFP powder was first mixed with PVDF and Super P in a 8:1:1 mass ratio. NMP was added to a desired viscosity and the solution was mixed in a planetary Thinky mixer for

20 min. The resulting slurry was coated onto aluminum foil using a doctor blade on an MTI laminate coater. The coated foil was then dried at 60 °C under vacuum overnight and punched into 12 mm electrodes with an average cathode mass loading of 3.5 mg/cm². The utilized mass loading is lower than typical commercial LIBs, >10 mg/cm², which allows for reduced transport resistances in our cathode. This enables greater isolation of the electrolyte's effect on kinetics and low-temperature performance. Lithium, a Celgard 2500 separator wetted with the electrolyte, and the LFP were inserted into CR-2032 coin cells, along with a 1.0 mm spacer, 0.5 mm spacer, and spring to apply constant stack pressure.

2.4. Electrochemical Characterization

Cycling studies were performed between 2.5 and 4.2 V vs. Li/Li⁺ with an Arbin BT-2000 Galvanostat. Cells were first formed with five full cycles at C/10. Electrochemical impedance spectroscopy (EIS) was conducted on lithium metal half cells that completed four full charge and discharge cycles, with a scanning range of 1 MHz to 0.01 Hz. Stainless steel symmetric cells were used to measure ionic conductivities through impedance spectroscopy from 25 °C to –40 °C. Lower temperature measurements, such as –50 °C, were limited by ice and impedance buildup in the circuit, limiting measurement accuracy. Linear sweep voltammetry (LSV) utilized a stainless steel || Li electrode setup while cyclic voltammetry used an LFP || Li half cell. For both CV and LSV, a 0.5 mV/s scan rate was utilized.

3. Results and Discussion

The developed gradient electrolytes consist of LiFSI salt, FEC, FEMC, NONA, and an experimental solvent, which is either diethylene carbonate (DEC), ethyl methyl carbonate (EMC), or dibutyl carbonate (DBC). The use of fluorinated carbonate solvents, FEC, and FEMC enables high ionic conductivity and an advantageous SEI formation [23]. The incorporation of NONA, which has an extremely low freezing point of –135 °C, significantly expands the electrolyte's liquid temperature range. LiFSI salt further enhanced SEI kinetics [22]. The electrolytes are abbreviated as F-FXFN, where X represents D for DEC, E for EMC, and B for DBC. As shown in Figure 1, The carbonate solvents have incrementally decreased dielectric constants of 89.6 for FEC, 9.56 for FEMC, and approximately 3.0 for DEC, EMC, and DBC. These gradient LHCEs were prepared using a 1 M LiFSI concentration with a 1:2:2:3 (FEC:FEMC:X:NONA) solvent volume ratio, and exhibited ultra-low freezing points below –120 °C. For comparison, we also prepared an electrolyte without the third coordinating solvent, abbreviated as F-FFN. This electrolyte was mixed in a 2:4:1 (FEC:FEMC:NONA) volume ratio. Both the gradient and F-FFN electrolytes' incorporation of the diluent, 37.5% and 14%, respectively, were near their respective miscibility limit.

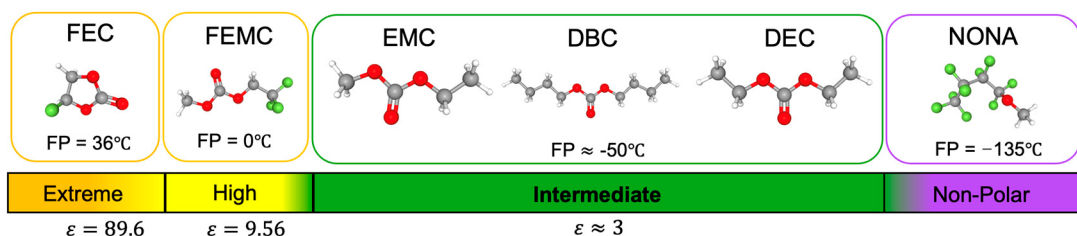


Figure 1. Graphical abstract of the step-down, gradient solvent design for localized high-concentrated electrolytes (FPs = freezing points).

To characterize these electrolytes, we thoroughly explored the solvation structure, electrochemical stability, and cell kinetics. Finally, we evaluated their effect on Li-metal cell performance, where the gradient LHCEs demonstrated superior low- and ultra-low-temperature performance compared to both commercial (COM) and F-FFN electrolytes.

3.1. Electrolyte Characterization

Raman spectroscopy was employed to characterize the behavior of anions within the electrolyte solvation shell. The spectra were deconvoluted to quantify the relative abundance of free anions (FSI^-)—those not coordinated in solution—contact-ion pairs (CIPs), which consist of shells with a single coordinating anion, and ion aggregates (AGGs), which contain two or more coordinating anions. The peaks corresponding to FSI^- , CIPs, and AGGs are observed at 720, 732, and 746 cm^{-1} , respectively [15]. The deconvoluted spectra and tabulated results are shown in Figure 2 and Table 1, respectively, for the experimental electrolytes.

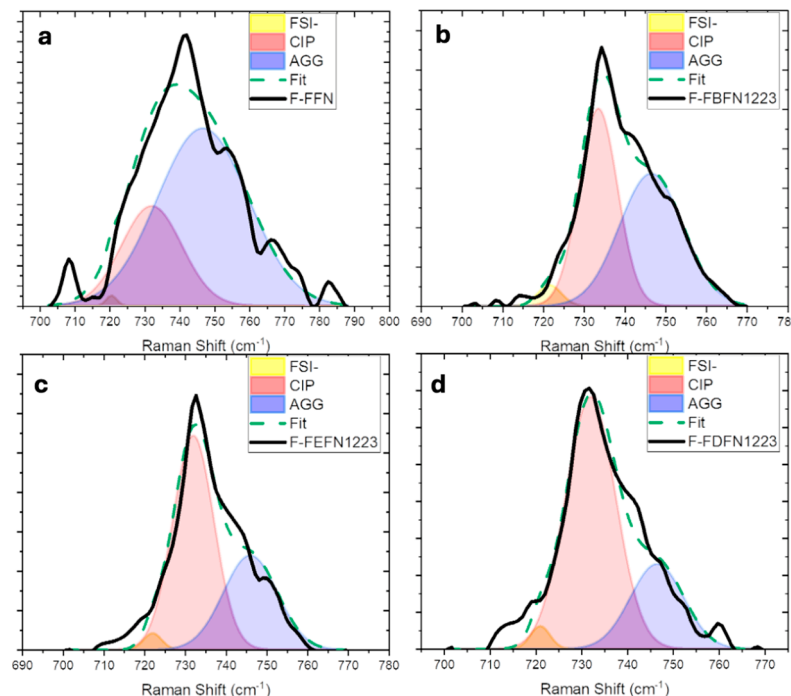


Figure 2. Solvation shell characterization with Raman spectroscopy for (a) F-FFN, (b) F-FBFN, (c) F-FEFN and (d) F-FDFN electrolytes.

Table 1. Relative abundance of FSI^- , CIPs, and AGGs for gradient and three-solvent electrolytes.

Electrolyte	FSI^- (%)	CIP (%)	AGG (%)
F-FFN	2	27	71
F-FDFN	2.4	71.8	25.6
F-FEFN	2	62.1	35.8
F-FBFN	3	46.2	50.7

The behavior of free FSI^- anions remain relatively consistent across both the gradient and F-FFN electrolytes, with 2–3% participation. This consistency suggests that anion participation in the solvation shell is preserved by adding the fourth solvent. However, the participation levels of CIPs and AGGs vary significantly. When comparing F-FFN to the gradient electrolytes, F-FFN exhibits a higher proportion of AGGs, with an integrated peak area of 71%. Among the gradient electrolytes, F-FDFN, F-FEFN, and F-FBFN show AGG peak areas of 25.6%, 35.8%, and 50.7%, respectively. The lower proportion of ion aggregates in the gradient electrolytes seems surprising given the reduced highly polar FEC content but may be explained by F-FFN's sterically simpler solvation structure [24,25]. The fourth solvent, EMC, DBC, or DEC, added to make F-FFN into the gradient electrolytes, are much bulkier molecules than FEC. In turn, this limits the amount of anion coordination possible, explaining the increased number of CIPs and reduced AGGs. When examining

the differences in AGGs within the different gradient electrolytes, steric effects no longer explain the trend. EMC and DEC have very similar and well-studied dielectric constants of 2.4 and 2.8, respectively [26,27]. DBC's dielectric constant is unavailable in the literature but is likely lower, <2.8, due to the larger alkyl chains. With this, the dielectric trend is inverse to the observed trend in AGG content. F-FDFN's lower AGG content is explained by DEC's stronger ability to solvate lithium ions and prevent aggregates. F-FEFN's AGG content is slightly higher than F-FDFN due to the slight decrease in dielectric constant from DEC to EMC. F-FBFN shows the greatest AGG content due to DBC's weaker solvating ability.

To characterize the electrolyte's electrochemical stability, cyclic voltammetry (CV) on $\text{Li} \parallel \text{LFP}$ half cells was performed from 2.5 V to 4 V at a scan rate of 0.5 mV/s (Figure A1a). After five cycles, the F-FDFN gradient LHCE shows a negligible, less than 10%, increase in the oxidation peak at 3.6 V and no change in the current density of the reduction peak at 3.25 V, indicating its electrochemical stability. Linear sweep voltammetry (LSV) was performed on $\text{Li} \parallel$ stainless steel cells, at a scan rate of 0.5 mV/s from OCV to 5 V (Figure A1b). All gradient LHCEs were stable up to 4.2 V. Above 4.2 V, the electrolytes show significant oxidation and current densities greater than the three-solvent, F-FFN, electrolyte, and much greater than the COM electrolyte. These results imply adequate stability for the gradient electrolytes within voltage limits for a $\text{Li} \parallel \text{LFP}$ cell. The gradient LHCE stability is further characterized later with long-term, low-temperature cycling studies.

3.2. Enhanced Kinetics

To investigate the effect of temperature on internal resistances and energy barriers, electrochemical impedance spectroscopy (EIS) was performed on $\text{LFP} \parallel \text{Li}$ half cells. Impedance measurements were taken at various temperatures ranging from -40°C to 20°C , with the frequency range spanning from 1 MHz to 0.01 Hz. Results were presented with Nyquist plots, where cell processes were observed across characteristic frequency ranges and modeled using the Randle's equivalent circuit (Figure A2). Through fitting the model, resistances associated with the desolvation–charge–transfer process (R_{CT}) and diffusion of lithium ions through the cathode solid-electrolyte interface (R_{SEI}) were calculated. After determining the resistances at different temperatures, the Arrhenius plots depicting R_{SEI} and R_{CT} across the temperature range were constructed (Figure 3a,b, respectively). Activation energies were then calculated by using linear regression and are shown in Table 2.

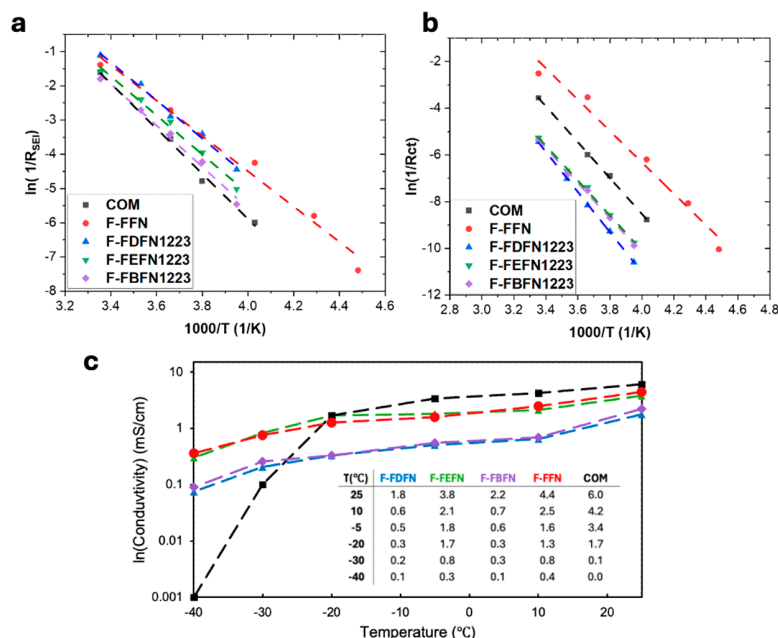


Figure 3. Kinetic characterizations of electrolytes with (a) Arrhenius plot for Li resistance through CEI, (b) Arrhenius plot for charge transfer process, and (c) ionic conductivity from 20 to -40°C .

Table 2. Activation energies for $E_{a,SEI}$ and $E_{a,CT}$ for gradient, three-solvent and COM electrolytes.

Electrolyte	$E_{a,SEI}$ (kJ/mol)	$E_{a,CT}$ (kJ/mol)
F-FFN	42.9	55.7
F-FDFN	46.2	59.6
F-FEFN	47.4	62.1
F-FBFN	50.3	62.4
COM	54.8	64.3

The three-solvent electrolyte, F-FFN, shows the lowest $E_{a,CT}$ at 55.7 KJ/mol. The gradient electrolytes all show greater $E_{a,CT}$ values, with F-FDFN, F-FEFN, and F-FBFN displaying values of 59.6, 62.1, and 62.3 kJ/mol, respectively. This result is expected considering F-FFN's greater contribution of AGG in its solvation shell, which lowers the desolvation energy. Similarly, $E_{a,SEI}$ follows the same trend: F-FFN has the lowest value, 42.8 kJ/mol, while F-FDFN, F-FEFN, and F-FBFN show values of 46.02, 47.4, and 47.4, respectively. This result once again reflects the F-FFN's increased AGG contribution and the more anion-derived SEI. Interestingly, F-FDFN shows lower $E_{a,CT}$ and $E_{a,SEI}$ despite having the smallest AGG peak. This observation contradicts the Raman data, which indicated that F-FDFN had the lowest AGG contribution. This discrepancy suggests that competing effects may influence the interfacial kinetics; F-FDFN's DEC content may offer advantages in SEI formation and desolvation.

In addition to characterizing Li SEI diffusion and charge transfer processes, the ionic conductivity of all electrolytes was measured (Figure 3c). EIS was performed on symmetric cells with stainless steel electrodes. The COM electrolyte demonstrated the highest ionic conductivity at -20°C and above, but its conductivity rapidly decreased at lower temperatures as it approached its freezing point. Interestingly, the F-FFN and F-FEFN electrolytes exhibited similar ionic conductivities, both of which were higher than F-FDFN's and F-FBFN's. Despite this small discrepancy, both the F-FFN and the gradient electrolytes followed a similar trend with temperature, maintaining ion mobility at -40°C and below.

3.3. Electrochemical Performance

Galvanostatic charge–discharge studies were performed on LiFePO₄ (LFP) || Li coin cells to evaluate the impact the electrolytes had on cell performance. Capacity retention through incremental temperature reductions, long-term low-temperature cycling, and ultra-low-temperature charge–discharge profiles are shown in Figure 4.

Figure 4a presents the capacity retention at -50°C , -40°C , -25°C , 0°C , and 25°C for the gradient, F-FFN, and COM electrolytes, all cycled at C/50. At 25°C and 0°C , all experimental electrolytes exhibit similar capacities of approximately 160 and 140 mAh/g, respectively. At 25°C , the gradient and F-FFN electrolytes outperform the commercial electrolyte. This arises from the improved interfacial kinetics, $E_{a,SEI}$ and $E_{a,CT}$, of the LHCEs while maintaining similar room-temperature ionic conductivities to COM electrolytes. Among the subzero temperatures, F-FDFN displayed the highest capacity, achieving 109.2 mAh/g at -50°C , which corresponds to 68% retention of its room-temperature capacity. Although F-FEFN and F-FBFN demonstrated lower subzero capacity retention compared to F-FDFN, they still outperformed F-FFN. F-FEFN and F-FBFN showed 97.2 and 92.2 mAh/g at -50°C , which corresponds to 60.1% and 58.5% retention, respectively. F-FFN showed a capacity of 88.2 mAh/g at -50°C , retaining 56% of its room-temperature capacity. In contrast, the COM electrolyte, while achieving high capacities at 25°C , experienced a significant decline at lower temperatures. Its capacity decreased from 111.6 mAh/g at 0°C to 42.1 mAh/g at -25°C .

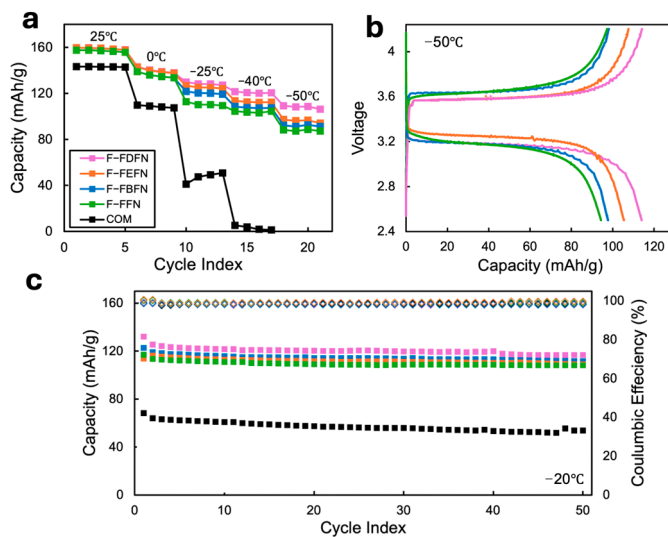


Figure 4. Performance of LFP || Li coin cells with F-FFN (green), F-FDFN (pink), F-FEFN (orange), F-FBFN (blue) and COM (black) electrolytes under various tests: (a) incremental temperature drop from 25 °C to −40 °C at C/50 rate; (b) charge–discharge curves at ultra-low-temperature, −50 °C and C/50 rate; and (c) discharge capacity and coulombic efficiency over many cycles at −20 °C and C/20.

Charge–discharge curves at ultra-low-temperature, −50 °C, and a C/50 rate are shown in Figure 4b. F-FDFN demonstrates the highest capacity, followed by F-FEFN, F-FBFN, and F-FFN. F-FDFN shows a capacity of 114.1 mAh/g with an overpotential of about 0.125 volts. With a similar overpotential is F-FEFN, but with slightly lower capacity of 105.5 mAh/g. The F-FBFN and F-FFN electrolytes exhibit similar polarizations of approximately 0.15 V, and capacities of 97.8 mAh/g and 94.3 mAh/g, respectively. The decreased overpotential correlates well with the $E_{a,SEI}$ values where F-FEFN and F-FDFN showed lower energy requirements than F-FBFN. This result could demonstrate an increased contribution of diffusion resistance to poor ultra-low-temperature performance. The COM electrolyte was unable to cycle at this temperature due to electrolyte freezing.

The long-term cyclability of the electrolytes was tested at −20 °C with a C/20 rate; the results are shown in Figure 4c. F-FDFN exhibited the highest capacity retention after 50 cycles, maintaining 116.8 mAh/g. All electrolytes, including COM, demonstrated stable cycling behavior and high coulombic efficiencies. F-FFN, F-FDFN, F-FEFN, F-FBFN, and the COM electrolyte recorded average coulombic efficiencies of 99.2%, 98.1%, 99.3%, 98.2%, and 98.4%, respectively. F-FEFN showed the best capacity retention, retaining 95.9% of its first cycle capacity on cycle 50. F-FFN was slightly behind at 92.6%. F-FDFN and F-FBFN showed capacity retentions of 88.4% and 90.9%, respectively, with COM far behind at 78.7%. This indicates that the gradient electrolytes form stable passivation layers and are not continuously consumed at the electrode surfaces. In contrast, the COM electrolytes' greater loss in capacity may be due to dendrite formation and subsequent electrolyte consumption, arising from its worse interfacial kinetics. Similarly, the F-FFN's greatest capacity retention may be explained; its interfacial kinetics are superior to that of the gradient electrolytes, suppressing dendritic growth. At −20 °C, the COM electrolyte showed less than half the capacity of the gradient electrolytes, with F-FDFN and the COM electrolyte achieving 116.8 mAh/g and 53.8 mAh/g, respectively, at cycle 50. The F-FDFN electrolyte once again showed superior capacity compared to F-FEFN and F-FBFN which showed 109.2 and 111.7 mAh/g, respectively. For all electrolytes, there is a minor change in capacity during the first three cycles, arising from electrolyte consumption and SEI formation. On cycle 40, F-FDFN has a slight drop from 120.0 mAh/g to 118.0 mAh/g. COM also has a gain in capacity, 51.9 mAh/g to 55.6 mAh/g on cycle 47. Both changes can be explained by minor dendritic growth and additional SEI growth on the lithium anode surface. Electrolyte

consumption could lead to both a temporary increase in capacity, in the case of COM, or a decrease in lithium reserve and subsequent capacity, in the case of F-FDFN.

All the gradient electrolytes demonstrated superior performance at low and ultra-low temperatures compared to the COM and F-FFN electrolyte. This result is despite having higher $E_{a,CT}$ and $E_{a,SEI}$ values and similar ionic conductivities. This result suggests that while improving interfacial kinetics is important, they do not solely determine low-temperature performance. The enhanced low-temperature performance of the gradient electrolytes can be attributed to their substantially lowered freezing point, achieved by incorporating 37.5% diluent by volume. Within the gradient electrolytes, the fourth solvent made a substantial difference in solvation shell, interfacial kinetics and subsequent performance.

4. Conclusions

Four solvent, gradient LHCEs were created, allowing for enhanced miscibility between extremely polar FEC and non-polar NONA. This improved miscibility allowed for 37.5% diluent by volume, which lowered the electrolyte freezing point below -120°C . Within the gradient LHCE design, three different solvents featuring intermediate dielectric constants and variable steric hindrance were investigated. The gradient LHCEs maintained a localized high salt concentration, shown by Raman spectroscopy with less than 3% free anion in the solution. In addition, an anion-derived SEI was shown by the reduced $E_{a,CT}$ and $E_{a,SEI}$ compared to the COM electrolyte. Due to the incorporation of FEC, room-temperature ionic conductivities similar to that of the EC-based COM electrolyte were observed, while the substantial incorporation of NONA ($\text{FP} = -135^{\circ}\text{C}$) allowed for ion mobility below -40°C . Within $\text{Li} \parallel \text{LFP}$ coin cells, all three gradient electrolytes outperformed both the three-solvent F-FFN electrolyte as well as a COM electrolyte. The F-FDFN gradient LHCE showed the best performance, retaining 68% of its 25°C capacity at -50°C . This electrolyte design shows a promising avenue for expanding the low-temperature operating range while maintaining advantageous room-temperature performance.

Author Contributions: Conceptualization, E.A.A. and J.S.P.; methodology, E.A.A.; formal analysis, J.S.P. and E.A.A.; investigation, J.S.P. and E.A.A.; resources, V.G.P.; data curation, J.S.P. and E.A.A.; writing—original draft preparation, J.S.P.; writing—review and editing, J.S.P., E.A.A. and V.G.P.; visualization, J.S.P. and E.A.A.; supervision, V.G.P.; project administration, V.G.P.; funding acquisition, V.G.P. All authors have read and agreed to the published version of the manuscript.

Funding: This research received no external funding.

Data Availability Statement: Data are available from the authors upon request.

Conflicts of Interest: The authors declare no conflicts of interest.

Appendix A

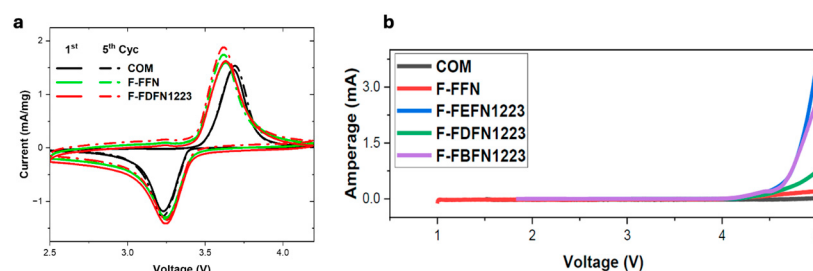


Figure A1. Electrochemical stability evaluated with (a) cyclic voltammetry, (b) linear sweep voltammetry on $\text{Li} \parallel \text{LFP}$ half cells. The gradient electrolytes all show similar electrochemical stability as the COM and F-FFN electrolytes, up to about 4 V.

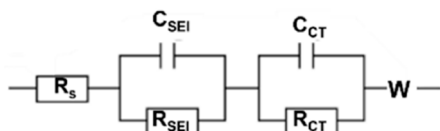


Figure A2. Equivalent Randles circuit used to evaluate charge transfer and SEI diffusion resistances.

References

- Chu, S.; Cui, Y.; Liu, N. The Path towards Sustainable Energy. *Nat. Mater.* **2017**, *16*, 16–22. [\[CrossRef\]](#) [\[PubMed\]](#)
- Hou, J.; Yang, M.; Wang, D.; Zhang, J. Fundamentals and Challenges of Lithium Ion Batteries at Temperatures between -40 and 60 $^{\circ}\text{C}$. *Adv. Energy Mater.* **2020**, *10*, 1904152. [\[CrossRef\]](#)
- Zhu, G.; Wen, K.; Lv, W.; Zhou, X.; Liang, Y.; Yang, F.; Chen, Z.; Zou, M.; Li, J.; Zhang, Y.; et al. Materials Insights into Low-Temperature Performances of Lithium-Ion Batteries. *J. Power Sources* **2015**, *300*, 29–40. [\[CrossRef\]](#)
- Feng, Y.; Zhou, L.; Ma, H.; Wu, Z.; Zhao, Q.; Li, H.; Zhang, K.; Chen, J. Challenges and Advances in Wide-Temperature Rechargeable Lithium Batteries. *Energy Environ. Sci.* **2022**, *15*, 1711–1759. [\[CrossRef\]](#)
- Zhang, N.; Deng, T.; Zhang, S.; Wang, C.; Chen, L.; Wang, C.; Fan, X. Critical Review on Low-Temperature Li-Ion/Metal Batteries. *Adv. Mater.* **2022**, *34*, 2107899. [\[CrossRef\]](#) [\[PubMed\]](#)
- An, Z.; Jia, L.; Ding, Y.; Dang, C.; Li, X. A Review on Lithium-Ion Power Battery Thermal Management Technologies and Thermal Safety. *J. Therm. Sci.* **2017**, *26*, 391–412. [\[CrossRef\]](#)
- Smart, M.C.; Ratnakumar, B.V.; Surampudi, S. Electrolytes for Low-Temperature Lithium Batteries Based on Ternary Mixtures of Aliphatic Carbonates. *J. Electrochem. Soc.* **1999**, *146*, 486. [\[CrossRef\]](#)
- Li, J.; Yuan, C.F.; Guo, Z.H.; Zhang, Z.A.; Lai, Y.Q.; Liu, J. Limiting Factors for Low-Temperature Performance of Electrolytes in LiFePO₄/Li and Graphite/Li Half Cells. *Electrochim. Acta* **2012**, *59*, 69–74. [\[CrossRef\]](#)
- Liao, X.-Z.; Ma, Z.-F.; Gong, Q.; He, Y.-S.; Pei, L.; Zeng, L.-J. Low-Temperature Performance of LiFePO₄/C Cathode in a Quaternary Carbonate-Based Electrolyte. *Electrochim. Commun.* **2008**, *10*, 691–694. [\[CrossRef\]](#)
- Zhang, S.S.; Xu, K.; Jow, T.R. A New Approach toward Improved Low Temperature Performance of Li-Ion Battery. *Electrochim. Commun.* **2002**, *4*, 928–932. [\[CrossRef\]](#)
- Zhang, S.S.; Xu, K.; Jow, T.R. The Low Temperature Performance of Li-Ion Batteries. *J. Power Sources* **2003**, *115*, 137–140. [\[CrossRef\]](#)
- Yamada, Y.; Furukawa, K.; Sodeyama, K.; Kikuchi, K.; Yaegashi, M.; Tateyama, Y.; Yamada, A. Unusual Stability of Acetonitrile-Based Superconcentrated Electrolytes for Fast-Charging Lithium-Ion Batteries. *J. Am. Chem. Soc.* **2014**, *136*, 5039–5046. [\[CrossRef\]](#)
- Suo, L.; Hu, Y.-S.; Li, H.; Armand, M.; Chen, L. A New Class of Solvent-in-Salt Electrolyte for High-Energy Rechargeable Metallic Lithium Batteries. *Nat. Commun.* **2013**, *4*, 1481. [\[CrossRef\]](#) [\[PubMed\]](#)
- Wang, J.; Yamada, Y.; Sodeyama, K.; Chiang, C.H.; Tateyama, Y.; Yamada, A. Superconcentrated Electrolytes for a High-Voltage Lithium-Ion Battery. *Nat. Commun.* **2016**, *7*, 12032. [\[CrossRef\]](#)
- Yamada, Y.; Yaegashi, M.; Abe, T.; Yamada, A. A Superconcentrated Ether Electrolyte for Fast-Charging Li-Ion Batteries. *Chem. Commun.* **2013**, *49*, 11194–11196. [\[CrossRef\]](#)
- Dong, X.; Lin, Y.; Li, P.; Ma, Y.; Huang, J.; Bin, D.; Wang, Y.; Qi, Y.; Xia, Y. High-Energy Rechargeable Metallic Lithium Battery at -70 $^{\circ}\text{C}$ Enabled by a Cosolvent Electrolyte. *Angew. Chem. Int. Ed.* **2019**, *58*, 5623–5627. [\[CrossRef\]](#) [\[PubMed\]](#)
- Chen, J.; Zhang, H.; Fang, M.; Ke, C.; Liu, S.; Wang, J. Design of Localized High-Concentration Electrolytes via Donor Number. *ACS Energy Lett.* **2023**, *8*, 1723–1734. [\[CrossRef\]](#)
- Yamada, Y.; Wang, J.; Ko, S.; Watanabe, E.; Yamada, A. Advances and Issues in Developing Salt-Concentrated Battery Electrolytes. *Nat. Energy* **2019**, *4*, 269–280. [\[CrossRef\]](#)
- Kim, S.; Seo, B.; Ramasamy, H.V.; Shang, Z.; Wang, H.; Savoie, B.M.; Pol, V.G. Ion–Solvent Interplay in Concentrated Electrolytes Enables Subzero Temperature Li-Ion Battery Operations. *ACS Appl. Mater. Interfaces* **2022**, *14*, 41934–41944. [\[CrossRef\]](#) [\[PubMed\]](#)
- Kim, S.; Pol, V.G. Tailored Solvation and Interface Structures by Tetrahydrofuran-Derived Electrolyte Facilitates Ultralow Temperature Lithium Metal Battery Operations. *ChemSusChem* **2023**, *16*, e202202143. [\[CrossRef\]](#)
- Jiang, L.-L.; Yan, C.; Yao, Y.-X.; Cai, W.; Huang, J.-Q.; Zhang, Q. Inhibiting Solvent Co-Intercalation in a Graphite Anode by a Localized High-Concentration Electrolyte in Fast-Charging Batteries. *Angew. Chem. Int. Ed.* **2021**, *60*, 3402–3406. [\[CrossRef\]](#) [\[PubMed\]](#)
- Adams, E.; Parekh, M.; Gribble, D.; Adams, T.; Pol, V.G. Novel Ternary Fluorinated Electrolyte’s Enhanced Interfacial Kinetics Enables Ultra-Low Temperature Performance of Lithium-Ion Batteries. *Sustain. Energy Fuels* **2023**, *7*, 3134–3141. [\[CrossRef\]](#)
- Cho, Y.-G.; Li, M.; Holoubek, J.; Li, W.; Yin, Y.; Meng, Y.S.; Chen, Z. Enabling the Low-Temperature Cycling of NMC || Graphite Pouch Cells with an Ester-Based Electrolyte. *ACS Energy Lett.* **2021**, *6*, 2016–2023. [\[CrossRef\]](#)
- Li, X.; Pan, Y.; Liu, Y.; Jie, Y.; Chen, S.; Wang, S.; He, Z.; Ren, X.; Cheng, T.; Cao, R.; et al. Understanding Steric Hindrance Effect of Solvent Molecule in Localized High-Concentration Electrolyte for Lithium Metal Batteries. *Carb. Neutrality* **2023**, *2*, 34. [\[CrossRef\]](#)
- Chen, Y.; Yu, Z.; Rudnicki, P.; Gong, H.; Huang, Z.; Kim, S.C.; Lai, J.-C.; Kong, X.; Qin, J.; Cui, Y.; et al. Steric Effect Tuned Ion Solvation Enabling Stable Cycling of High-Voltage Lithium Metal Battery. *J. Am. Chem. Soc.* **2021**, *143*, 18703–18713. [\[CrossRef\]](#)

26. Ue, M.; Mori, S. Mobility and Ionic Association of Lithium Salts in a Propylene Carbonate-Ethyl Methyl Carbonate Mixed Solvent. *J. Electrochem. Soc.* **1995**, *142*, 2577. [[CrossRef](#)]
27. McEwen, A.B.; McDevitt, S.F.; Koch, V.R. Nonaqueous Electrolytes for Electrochemical Capacitors: Imidazolium Cations and Inorganic Fluorides with Organic Carbonates. *J. Electrochem. Soc.* **1997**, *144*, L84. [[CrossRef](#)]

Disclaimer/Publisher's Note: The statements, opinions and data contained in all publications are solely those of the individual author(s) and contributor(s) and not of MDPI and/or the editor(s). MDPI and/or the editor(s) disclaim responsibility for any injury to people or property resulting from any ideas, methods, instructions or products referred to in the content.